Theoretical investigation of magnetic anisotropy at the $La_{0.5}Sr_{0.5}MnO_3/LaCoO_{2.5}$ interface

Xiaobing Chen,[1,2] Shihao Zhang,[1,2] Banggui Liu,[1,2] Fengxia Hu,[1,2,3] Baogen Shen,[1,2,3] and Jirong Sun ![ORCID][1,2,3,4,*]

[1]*Beijing National Laboratory for Condensed Matter Physics & Institute of Physics, Chinese Academy of Sciences, Beijing 100190, People's Republic of China*
[2]*School of Physical Sciences, University of Chinese Academy of Sciences, Beijing 100049, People's Republic of China*
[3]*Songshan Lake Materials Laboratory, Dongguan, Guangdong 523808, People's Republic of China*
[4]*Spintronics Institute, University of Jinan, Jinan, Shandong 250022, People's Republic of China*

Based on density functional theory calculations, we show how symmetry mismatch at interface induces perpendicular magnetic anisotropy (PMA) for the perovskite/brownmillerite-typed $La_{1/2}Sr_{1/2}MnO_3/LaCoO_{2.5}$ superlattices in different strain states. We found strong interfacial reconstructions, which result in considerable orbital hybridization due to distortion/tilting of the MnO_6 octahedron and CoO_4 tetrahedron. We identified the orbital pairs that strongly affect magnetic anisotropy, showing that tuning the degree of orbital hybridization by lattice strain is an effective approach to tune magnetic anisotropy. Remarkably, not only octahedron-coordinated Mn ions but also tetrahedron-coordinated Co ions contribute to PMA. This work presents a guidance for tuning spin orientation by interface engineering.

I. INTRODUCTION

Perpendicular magnetic anisotropy (PMA) plays an important role in spintronics. It is highly desired by data storage and logical operation with high density, high stability and low energy consumption [1–4]. It is well known that the magnetic anisotropy stems from spin orbit coupling (SOC) that links the electron orbital with electron spin, i.e., crystallographic symmetry with magnetic moment [5,6]. Therefore, enhanced SOC and reduced crystal symmetry are two effective tactics to obtain strong PMA [7–9].

Perovskite oxides are promising spintronic materials since their electronic, magnetic, and structural properties are susceptible to the tilting/distortion of oxygen octahedra. Among them, $(La, Sr)MnO_3$ (LSMO), a double exchange ferromagnet when the content of Sr situates between 0.2 and 0.5 [10], is an intriguing system with tunable magnetic anisotropy. An ordinary way to amend the magnetic easy axis is to tune the epitaxial strain of the LSMO film. Accompanying the compressive to tensile strain transition, the magnetic easy axis changes from the out-of-plane to the in-plane direction, with a PMA constant of 10^4–10^5 erg/cm^3 [11,12]. It is a magnetoelastic effect. For perovskite oxide, tilting oxygen octahedron is also an effective way to tune magnetic anisotropy. As reported, by transferring octahedron rotation from $NdGaO_3$ to LSMO, an in-plane switching of the magnetic easy axis by an angle of 90° has been achieved for ultrathin films [13]. In this vein, anisotropic double exchange along two in-plane directions results in magnetic anisotropy. A third approach to obtain magnetic anisotropy is interlayer coupling. It has been recently shown that sandwiching the LSMO layer between two brownmillerite $LaCoO_{2.5}$ (LCO) layers can cause a PMA even if the LSMO layer is in a tensile

state that disfavors PMA [14]. The PMA constant achieved in this way is larger by two orders of magnitude than that resulted by compressive lattice strains or oxygen octahedron tilting [13]. This work demonstrates the great potential of interface engineering using oxides with different symmetries. However, it remains elusive how symmetry mismatch at perovskite/brownmillerite (P/B) interface induces the PMA and what are the key factors that determine the PMA. A thorough understanding of these issues will give us the capability to gain a distinct effect through interface engineering. In this paper, we present a systematic investigation of the magnetic anisotropy of the P/B superlattice in different strained states, adopting *ab initio* electronic structure calculations and second order perturbation theory. It was found that, due to symmetry mismatch, interfacial reconstructions marked by an elongation of MnO_6 octahedron and a deviation of CoO_4 from standard tetrahedron take place, resulting in orbital reconstruction inducing PMA. The element and orbital resolved magnetic anisotropy energy (MAE) were determined. Remarkably, not only octahedron-coordinated Mn ions but also tetrahedron-coordinated Co ions contribute to PMA. Combining the d electron configuration and the crystal field, a conceptual picture of PMA induced at the P/B interface is given.

II. COMPUTATIONAL DETAILS

We used density functional theory (DFT) calculations within the projected augmented-wave (PAW) method [15] as implemented in the Vienna *ab initio* simulation package (VASP) [16,17] code to investigate the P/B interface. The generalized gradient approximation of the Perdew-Burke-Ernzernhof modified for solids formalism [18,19] was adopted for exchange-correlation energy. A 500-eV kinetic energy cutoff was found to achieve numerical convergence. We adopted a k-point set generated by the $9 \times 9 \times 3$ Γ-centered Monkhorst-Pack mesh. More information about the

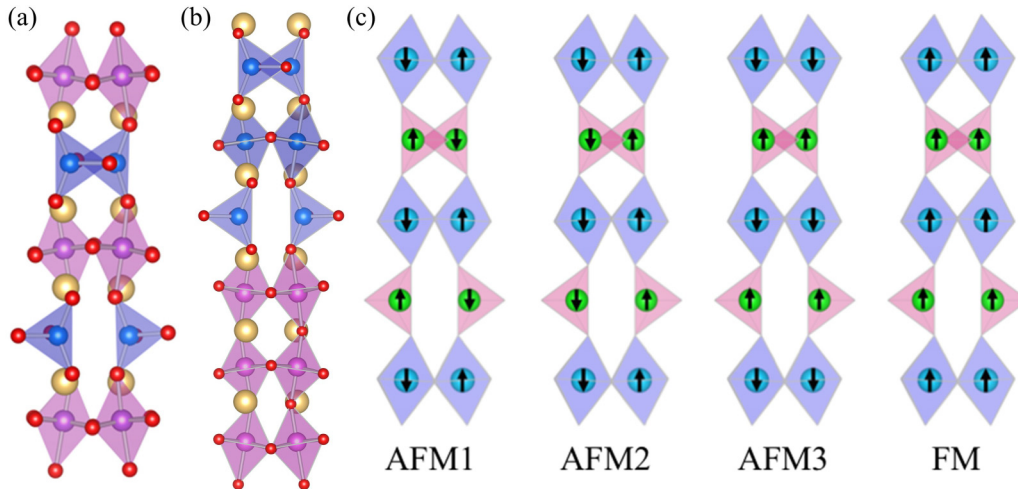*Corresponding author: jrsun@iphy.ac.cn

FIG. 1. Atomic structures of LSMO/LCO (a) (1,1) and (b) (3,3) superlattices for DFT calculations. La/Sr, Co, Mn, and O atoms are depicted as yellow, light-blue, magenta, and red spheres, respectively. For the (3,3) model, the Sr content in LSMO was set to the optimal level of 1/3, and different La/Sr configurations do not affect the main results. The results of the (3,3) superlattice are shown in Supplemental Material Fig. S2 [20]. (c) Possible in-plane spin orders in (1,1) superlattices.

k-point set convergence test can be seen in Fig. S1 of the Supplemental Material [20]. To study the effect of electron correlation, the DFT+U approach within the rotationally invariant formalism and the double-counting formula was performed with $U_{eff} = 3.0$ and 3.3 eV for Mn and Co 3d orbitals, respectively [21–23]. Atomic positions were optimized until the Hellman-Feynman force on each atom was smaller than 0.01 eV/A and the electronic iteration was performed until the total energy change was smaller than 10^{-5} eV. Additionally, the SOC calculation was implemented in VASP in a noncollinear mode [24,25], which allows a self-consistent calculation of orbital moments and magnetic anisotropy energy. MAE was the energy gained by rotating the direction of magnetic moment from the $x-y$ plane ($E_{\parallel}$) to the z axis ($E_{\perp}$), i.e., MAE is the magnetic anisotropic energy. To get an accurate determination of the MAE, a self-consistency convergence within 10^{-8} eV and a dense k-point mesh of 13 $\times$ 13 $\times$ 5 has been achieved in our calculations. In addition, the element and orbital resolved MAE are obtained from the difference between the SOC energies along the in-plane and out-of-plane directions, $\Delta E_{soc} = E_{soc\parallel} - E_{soc\perp}$. Here $E_{soc} = \langle \frac{\hbar^2}{2m^2c^2} \frac{1}{r} \frac{dV}{dr} \hat{L} \cdot \hat{S} \rangle$, where $V(r)$ is the spherical part of the effective potential within the PAW sphere, and L and S are the orbital and spin angular momentums, respectively. E_{soc} is twice the actual value of the total energy correction associated with SOC to second order, i.e., MAE $\approx \frac{1}{2} \Delta E_{soc}$ [26,27]. The other half of the SOC energy translates into the crystal-field energy and the formation energy of the unquenched orbital moments [28].

III. RESULTS AND DISCUSSION

A. Atomic and magnetic structure of superlattice

To highlight the effect of MnO$_6$-CoO$_4$ interlayer coupling on magnetic anisotropy for the P/B interface and to save computing time, the system was modeled by a brownmillerite-structured superlattice consisting of (CoO$_4$)$_1$/(MnO$_6$)$_1$

without vacuum layer as shown in Fig. 1(a) [29]. In our (1,1) superlattice, the A site atom is La for the CoO$_4$ layer and half La and half Sr for the MnO$_6$ layer. This yields the smallest supercell, which captures the main feature of the effect of interlayer coupling for the P/B-typed superlattice. We also investigated a (LCO)$_3$/(LSMO)$_3$ supercell model without vacuum layer as shown in Fig. 1(b) to further verify interfacial effect and obtained the same conclusion that the P/B interface played a key role in determining PMA as for the (1,1) system (Supplemental Material Fig. S2 [20]). Therefore, the results below were obtained mainly for the (1,1) model.

During the DFT calculations, the equilibrium bulk lattice constant of LSMO was set to the experimental value of $a_0 = 3.865$ Å [30], and the in-plane lattice constant of the superlattice ($a_{\parallel}$) was set to that of the substrate. In this case, the biaxial strain was defined by $\varepsilon = (a_{\parallel}-a_0)/a_0 \times 100\%$. The magnetic ground states of bulk LCO and LSMO are A-type antiferromagnetic (A-AFM) and ferromagnetic (FM), respectively [14]. To identify the most stable magnetic phase in superlattice, we considered a FM and three AFM configurations [Fig. 1(c)]. The calculated total energies under different strains are presented in Table I, with respect to that of the AFM3 configuration. Evidently, the AFM3 state with

TABLE I. Calculated total energies for the magnetic configurations in (1,1) superlattice (in the unit of meV per 1 $\times$ 1 supercell). The total energies of AFM3 are set to zero. -2% and 4% correspond to the lattice strains of LSMO on LaAlO$_3$ and BaTiO$_3$, respectively.

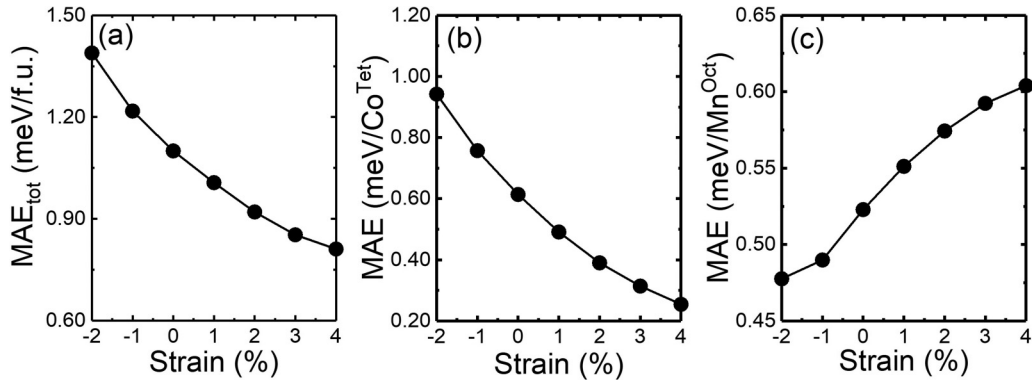| ε	AFM1	AFM2	AFM3	FM
-2%	47.5	86.8	0.0	48.4
-1%	52.9	93.7	0.0	45.7
0%	55.3	96.0	0.0	45.3
$+1\%$	56.9	96.6	0.0	43.6
$+2\%$	58.3	96.8	0.0	41.8
$+3\%$	59.4	96.2	0.0	39.6
$+4\%$	60.8	95.7	0.0	37.3

FIG. 2. Strain dependence of (a) total MAE, (b) element resolved MAE per Co atom, and (c) element resolved MAE per Mn atom.

antiparallel spins in neighboring MnO_6 and CoO_4 is most stable. In contrast, FM, AFM1, and AFM2 have much higher energies than AFM3. Model AFM3 is consistent with the experimental results for LSMO/LCO superlattice for which signatures of antiparallel spin alignment between LSMO and LCO have been observed [14]. The magnetic moments of Mn and Co converge to ∼3.9 and ∼2.6 μ_B, respectively, which agrees well with the previous report [29,31]. The latter value is close to the magnetic moment of a high spin Co^{2+} ion with d^7 configuration ($S = 3/2$) that has an expected local magnetic moment of $3\mu_B$. Lattice strains only cause a slight variation in magnetic moment ($<1\%$), which rules out spin state transition in Co ions suffering from lattice strains (not shown). For the (3,3) superlattice, we find that the coupling between Co^{Tet} (Co ion caged by a CoO_4 tetrahedron) and Mn^{Oct} (Mn ion in a MnO_6 octahedron) is also AFM [29], indicating that the (1,1) model indeed captures the main features of the P/B superlattice.

B. Magnetic anisotropy energy

Now we turn to the discussion about the MAE in different strain states. The total MAE and element resolved MAE calculated within the noncollinear self-consistent calculations are shown in Figs. 2(a)–2(c) for the (1,1) superlattice with the biaxial strains ranging from −2% to 4%. As shown in Fig. 2(a), the maximal MAE is 1.4 meV/f.u. (1.9×10^7 erg/cm³), gained under a compressive strain of −2%. As lattice strain grows from −2% to 4%, MAE smoothly decreases to 0.8 meV/f.u. (1.0×10^7 erg/cm³). Positive MAE implies PMA. For the superlattice on STO ($\varepsilon \approx 1\%$), the corresponding PMA constant is 1.3×10^7 erg/cm³, close to the experimental value reported for the LSMO/LCO superlattice [14]. Fascinatingly, PMA remains strong even if under a tensile strain as large as +4%. This is in sharp contrast to the bare LSMO film which shows an in-plane magnetic anisotropy in tensile strain state.

To learn more about the contribution from different atoms, element resolved MAE was further calculated. As illustrated in Fig. 2(b), the MAE per Co atom is 0.94 meV, gained under the strain of −2%. As lattice strain grows from −2% to 4%, it decreases from 0.94 to 0.26 meV. For Mn, the element resolved MAE varies from 0.46 to 0.63 meV/Mn [Fig. 2(c)], slightly growing with lattice strain. These results are striking. They show that not only LSMO but also LCO layer contributes to PMA; the PMA comes mainly from Co

ions under strong compressive strains and Mn ions under tensile strains. The magnetically easy z axis and hard xy plane for CoO_4 tetrahedra are consistent with previous reports on $SrCoO_{2.5}$ [32]. Notably, the obtained MAE per Co atom is one order of magnitude greater than that previously observed in CoO_4 tetrahedra [33]. We also calculated the magnetic anisotropy for a bare LSMO layer and obtained the MAEs of 0.019, −0.036, and −0.141 meV/Mn, corresponding to lattice strains of −2%, +1%, and +4%. The calculated MAE for the compressive strain of −2% is close to the reported value for the LSMO film grown on $LaAlO_3$ [34]. Notably, the MAE here is not only much smaller in magnitude than that of the LSMO layer in the P/B superlattice but also negative when tensely strained. Obviously, the PMA of the P/B superlattice is not a simple sum of that of the bare LCO and LSMO layers, and symmetry mismatch and interlayer coupling have greatly enhanced magnetic anisotropy.

We also calculated the anisotropy energy between two in-plane directions, [100] and [110] and found that the difference for Mn is nearly zero, suggesting the in-plane tetragonal symmetry of MnO_6. In contrast, the MAE difference is nearly 10% for Co between [100] and [110], indicating an in-plane anisotropy for CoO_4.

In addition to SOC, the anisotropy caused by dipole-dipole interaction also will contribute to MAE, resulting in shape anisotropy. We used $E_{sh} = -2\pi M_s^2$ to get a simplified expression for shape anisotropy energy in magnetic superlattice [35] and found that E_{sh} is about -10^5 erg/cm³ (-0.01 meV/Mn). This is a reasonable value consistent with that derived from the dipole-dipole interaction [36] but much smaller than electronic contributions. Therefore, the magnetic anisotropy is mainly determined by SOC, i.e., MAE ≈ MCA, where MCA is magnetocrystalline anisotropy energy.

MAE can also be derived from the force theorem [37], a second order perturbation theory-based method. Adopting the torque method, we obtained similar strain dependence of the MAE on lattice strain, which confirms the strong PMA of the P/B interface. The value of MAE calculated by the force theorem is half the result of self-consistent calculations. This is an intrinsic difference between these two approaches. The MAE values as a function of strain using the force theorem is shown in Fig. S3 of the Supplemental Material [20]. We also calculated the strain dependence of MAE for the (3,3) superlattice adopting the force theorem and obtained results
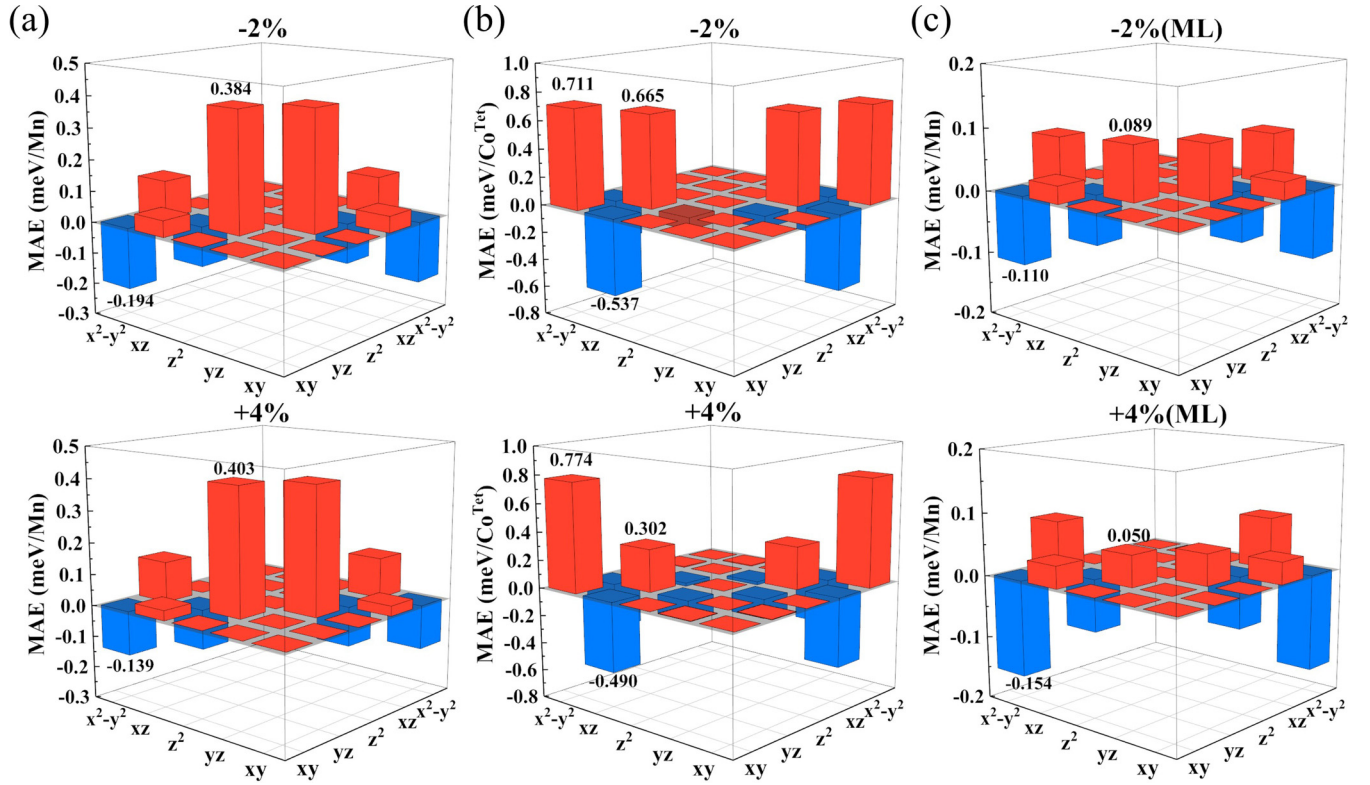
FIG. 3. Contributions to MAE from the SOC interaction between different d orbital spin channels for (a) Mn, (b) Co atoms at the P/B interface, and (c) Mn in a bare LSMO film under selected lattice strains of -2% and $+4\%$.

similar to those of the (1,1) superlattice. A detailed overview of the comparison between different superlattice can be found in Supplemental Material Fig. S2 [20].

C. Orbital resolved magnetic anisotropy energy

Usually, the strongest effect comes from the lift of degeneracy of two orbital states by SOC with respect to the magnetization directions, i.e., the "hot spots" in the band structure [38,39]. The band structures for the (1,1) the P/B interface with in-plane and out-of-plane magnetization directions are shown in Fig. S4 of the Supplemental Material [20]. It is obvious that band structures in these two cases are very similar, implying the absence of "hot spots" that determine magnetic anisotropy. Since the orbitals close to the Fermi level are highly hybrid at the asymmetric the P/B interface, we believe that many minor differences in band structure contribute to the overall magnetic anisotropy rather than the "hot spots". We therefore adopted the orbital resolved MAE method to analyze the source of magnetic anisotropy at the P/B interface.

To find out the key factors that affect magnetic anisotropy, we calculated the d-orbital-projected contributions to MAE for the Mn and Co atoms. For this purpose, we translated $\hat{H}_{\text{SOC}} = \xi\hat{L}\cdot\hat{S}$ into $\hat{H}_{\text{SOC}} = \hat{H}^0_{\text{SOC}} + \hat{H}'_{\text{SOC}}$ [40,41], with the spin-conserving term

$$\hat{H}^0_{\text{SOC}} = \xi\hat{S}_{z'}\left(\hat{L}_z\cos\theta + \tfrac{1}{2}\hat{L}_+e^{-i\varphi}\sin\theta + \tfrac{1}{2}\hat{L}_-e^{i\varphi}\sin\theta\right), \quad (1)$$

and the spin-non-conserving term

$$\hat{H}'_{\text{SOC}} = \frac{\xi}{2}\hat{S}_{+'}\left(-\hat{L}_z\sin\theta - \hat{L}_+e^{-i\varphi}\sin^2\frac{\theta}{2} + \hat{L}_-e^{i\varphi}\cos^2\frac{\theta}{2}\right)$$

$$+ \frac{\xi}{2}\hat{S}_{-'}\left(-\hat{L}_z\sin\theta + \hat{L}_+e^{-i\varphi}\cos^2\frac{\theta}{2} - \hat{L}_-e^{i\varphi}\sin^2\frac{\theta}{2}\right), \quad (2)$$

where ξ is the SOC coefficient, θ and φ are the azimuthal and polar angles of the spin orientation with respect to the local coordinate environment, and $\hat{L}_{x(z)}$ is the $x(z)$ component of the orbital angular momentum operator. By treating the SOC Hamiltonian as a perturbation, we can get the associated energy correction by SOC, i.e., the quantitative value of MAE,

$$\text{MAE} = \xi^2\sum_{u,o,\sigma,\sigma'}(-1)^{1-\delta_{\sigma\sigma'}}\left[\frac{|\langle o^{\sigma'}|\hat{L}_z|u^\sigma\rangle|^2 - |\langle o^{\sigma'}|\hat{L}_x|u^\sigma\rangle|^2}{\varepsilon_u^\sigma - \varepsilon_o^{\sigma'}}\right], \quad (3)$$

where $u^\sigma(o^{\sigma'})$ and $\varepsilon_u^\sigma(\varepsilon_o^{\sigma'})$ stand for the eigenstate and eigenvalue of unoccupied (occupied) orbital state d_{xy}, d_{yz}, d_{z^2}, d_{xz}, or $d_{x^2-y^2}$, respectively (here s and p orbitals have been omitted because of their neglibigle contributions), $\sigma(\sigma')$ represent spin state, and δ is the kronecker function.

On the basis of Eq. (3), we are able to analyze the contributions of all possible orbit combinations of Mn and Co. Fig. 3(a) shows the MAE corresponding to all orbital pairs for the Mn in the P/B superlattice. From first glance, the MAE is mainly determined by two matrix elements, i.e., $\langle d_{z^2}|\hat{L}_z|d_{yz}\rangle$
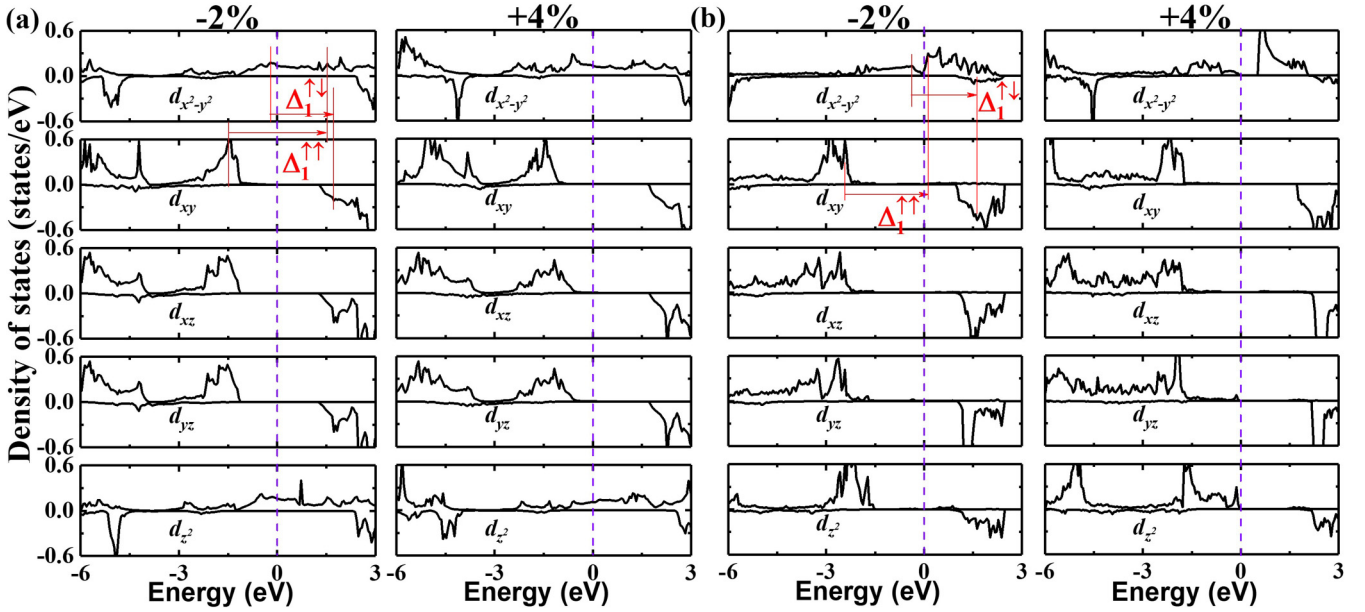
FIG. 4. PDOS of d orbitals of the Mn atoms in (a) LSMO bare film ($x = 1/2$) and (b) (1,1) superlattice under selected strains of -2% and $+4\%$. The Fermi energy is indicated by a vertical dashed line. Triangles mark the energy difference between different orbital states for selected orbital pairs.

and $\langle d_{x^2-y^2}|\hat{L}_z|d_{xy}\rangle$. The former orbital pair yields a positive MAE, which means that the occupation of the d_{z^2} state always supports PMA. In contrast, the latter term is negative, i.e., the occupied $d_{x^2-y^2}$ orbit favors an in-plane magnetic anisotropy. Since the contribution from the first term is considerably larger than that from the second one in magnitude, the total MAE is positive, i.e., Mn exhibits a PMA. Moreover, the MAEs from these two orbital pairs display different dependence on lattice strain. Accompanying the compressive to tensile transition, the first term slightly increases whereas the second term considerably decreases in magnitude. Consequently, MAE grows sizably with lattice strain [Fig. 2(c)]. This kind of strain dependence is unusual. In general, the contribution from $\langle d_{z^2}|\hat{L}_z|d_{yz}\rangle$ or $\langle d_{x^2-y^2}|\hat{L}_z|d_{xy}\rangle$ should be depressed or enhanced by tensile strains, which will cause a compression of the MnO_6 octahedron along the z axis. This is exactly what we observed in the LSMO monolayer. Corresponding to the increase of lattice strain from -2% to $+4\%$, as shown in Fig. 3(c), the contribution from $\langle d_{z^2}|\hat{L}_z|d_{yz}\rangle$ decreases by a factor of 1.8 whereas that from $\langle d_{x^2-y^2}|\hat{L}_z|d_{xy}\rangle$ grows from -0.110 to -0.154 meV/Mn. As a result, the LSMO monolayer transits from PMA to easy plane anisotropy, in agreement with experimental results. As will be seen later, interfacial reconstruction marked by atomic reconfiguration and orbital hybridization is responsible for the unusual PMA of the P/B superlattice.

To get a deeper insight into the abnormal MAE of the P/B superlattice, we analyzed the spin decomposed projected density of states (PDOS) of the d orbitals of Mn in the P/B superlattice and LSMO monolayer. As shown in Fig. 4, both the $d_{x^2-y^2}$ and d_{z^2} orbtials are occupied. This feature is observed not only in LSMO film but also in the P/B superlattice. It is indicative of strong lattice distortion of the MnO_6 octahedra, which causes a mixing of the two e_g orbital states. As a consequence of orbital mixing, the d_{z^2} and $d_{x^2-y^2}$

bands are conductive for the LSMO film [(Fig. 4(a)]. This is consistent with the observation that the LSMO film is metallic. As expected, the t_{2g} orbitals locate well below Fermi level, without any signatures of orbital hybridization between Mn t_{2g} and O $2p$ orbitals. Accompanying the transition from compressive to tensile strains, t_{2g} and e_g orbitals (mainly the latter orbital) redistribute. Through integrating the density of states below Fermi level in Fig. 4(a), we find the electron occupancy ratio of d_{z^2} to $d_{x^2-y^2}$ varies from 1.042 to 0.920 as lattice strain grows from -2% to 4% (Details about electron occupation ratio are shown in Table SI of the Supplemental Material [20]). The electron population of the $d_{x^2-y^2}$ band increases at the compensation of that of the d_{z^2} band. This is understandable since tensile strain will increase the space between in-plane Mn and O atoms, thus lowering the $d_{x^2-y^2}$ orbitals via reducing the Coulomb repulsion among electrons. Compared with LSMO, however, the P/B superlattice owns a different band structure. As shown in Fig. 4(b), a finite energy gap develops between the occupied spin-up d_{z^2} band and the unoccupied spin-down d_{z^2} band around Fermi level. Consequently, the d_{z^2} orbital becomes strongly localized. More than that, orbital mixing is significantly modified, especially unoccupied states: The spin-up unoccupied e_g states have only the $d_{x^2-y^2}$ composition now [Fig. 4(b)] whereas they are $d_{x^2-y^2}$ and d_{z^2} mixed states for a bare LSMO film [Fig. 4(a)]. These results suggest the difference of the MnO_6 distortions in the P/B superlattice and LSMO film. As will be seen later, an enhanced elongation along the z axis emerges for the MnO_6 of the P/B superlattice, causing a large splitting of the two e_g orbitals.

Obviously, the strong PMA must have a close relationship with the distinct band structure of the P/B superlattice. According to Eq. (3), orbital resolved MAE is mainly determined by the energy difference between occupied and uoccupied orbital pairs. Take the $d_{z^2} - d_{yz}$ orbital pair as an
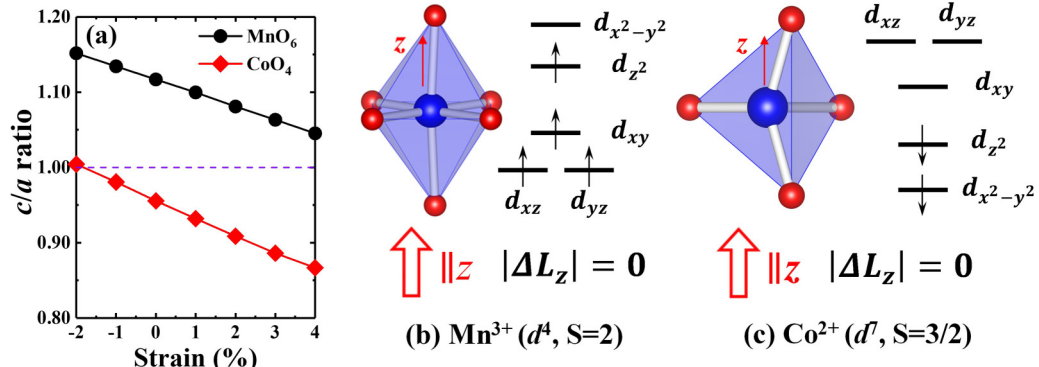
FIG. 5. (a) Calculated c/a ratio in MnO_6 and CoO_4 coordination. The purple dashed line represents the cubic state. (b) The spin-up electron configuration of $Mn^{3+}(3d^4, S=2)$ at a z-elongated octahedral site. (c) The spin-down electron configuration of $Co^{2+}(3d^7, S=3/2)$ at a z-contracted tetrahedral site. Both spin configurations are consistent with our calculated density of states shown in Supplemental Material Fig. S5 [20].

example. For LSMO, a positive term $\langle d_{z^2\uparrow}|\hat{L}_z|d_{yz\downarrow}\rangle$ and a negative term $\langle d_{yz\uparrow}|\hat{L}_z|d_{z^2\uparrow}\rangle$ emerge simultaneously since the the unoccupied spin-up states are the d_{z^2} and $d_{x^2-y^2}$ mixed states, and their counteraction makes the $\langle d_{z^2}|\hat{L}_z|d_{yz}\rangle$ term considerably low. For the P/B superlattice, in contrast, the unoccupied spin-up states are simply $d_{x^2-y^2}$ in nature due to the presence of an energy gap in the d_{z^2} band. In this case, only the positive term $\langle d_{z^2\uparrow}|\hat{L}_z|d_{yz\downarrow}\rangle$ survives, contributing to $\langle d_{z^2\uparrow}|\hat{L}_z|d_{yz}\rangle$. As a result, the matrix element $d_{z^2\uparrow}|\hat{L}_z|d_{yz\downarrow}$ is considerably large. This explains the large change in magnetic anisotropy from the P/B interface to LSMO monolayer (The $\langle d_{xy}|\hat{L}_z|d_{x^2-y^2}\rangle$ term does not change obviously from LSMO to the P/B superlattice as the $d_{x^2-y^2}$ band stay metallic).

For an ideal CoO_4 tetrahedron for which the Co^{2+} ion shows the $e_g^{2\uparrow}t_{2g}^{3\uparrow}e_g^{2\downarrow}t_{2g}^{0\downarrow}$ orbital states only two matrix elements are expected, a positive $\langle d_{x^2-y^2\downarrow}|\hat{L}_z|d_{xy\downarrow}\rangle$ and a negative $\langle d_{xy\downarrow}|\hat{L}_x|d_{xz\downarrow}\rangle$ (refer to Sec. III D for details). According to Fig. 3(b), however, there are three matrix elements that contribute to MAE for the Co ions in superlattice, i.e., $\langle d_{x^2-y^2\downarrow}|\hat{L}_z|d_{xy\downarrow}\rangle$, $\langle d_{xz\downarrow}|\hat{L}_z|d_{yz\downarrow}\rangle$, and $\langle d_{xy\downarrow}|\hat{L}_x|d_{xz\downarrow}\rangle$. The former two terms are positive while the last one is negative. A further analysis of the band structure indicates that the additional term could be ascribed to lattice distortion-induced orbital hybridization. As will be shown later, the CoO_4 tetrahedra are strongly distorted, deviating by a large angle away from the custom z direction. This in turn causes a strong Co $3d$ - O $2p$ hybridization due to the charge transfer between Co and in-plane surrounding oxygen atoms [29]. As a consequence, the occupied spin-down $d_{x^2-y^2}$ and d_{z^2} states are mixed with the unoccupied spin-down d_{xz} and d_{yz} states via SOC, then the spin-down states are all partially occupied as shown in Fig. S5 of the Supplemental Material [20]. This gives rise to a positive $\langle d_{xz\downarrow}|\hat{L}_z|d_{yz\downarrow}\rangle$ term that contributes to the magnetic anisotropy of Co. Since the orbital hybridization depends strongly on the degree of the CoO_4 distortion, the $\langle d_{xz\downarrow}|\hat{L}_z|d_{yz\downarrow}\rangle$ matrix element thus MAE vary significantly with lattice strains [shown in Fig. 2(b)].

For a comparison investigation, we also calculated the MAE with the SOC constant. According to Bruno formula, MAE $= -\frac{\xi}{4\mu_B}\Delta\mu_L$ [42], MAE values of $0.18 \sim 0.23$ meV are obtained as the strain grows from -2% to $+4\%$, adopt-

ing the DFT calculated $\Delta\mu_L = 0.016 \sim 0.021\,\mu_B$ and the extrapolated $\xi_{Mn} = 0.044$ eV as reported by Francisco *et al.* [43]. They are different from the results obtained by DFT calculations [Fig. 2(c)]. Since the Bruno formula gives the MAE based on the orbital anisotropy in atomic spheres, this difference indicates that the magnetic anisotropy of the Mn ions at the P/B interface has implications more than orbital moment anisotropy. Probably, the strong orbital hybridization and the spin orbit coupling with Co ($\xi_{Co} = 0.07$ eV [43]) cannot be ignored. In other words, the off-site spin orbit coupling related spin-flip term may considerably affect the MAE at interface [44,45]. For Co^{Tet} ion, we also calculate the MAE with the SOC constant based on the Bruno formula, and the MAE turns out to be $0.9 \sim 0.3$ meV, consistent with the results in Fig. 2(b).

D. A conceptual picture for enhanced PMA

From the above results, the MAE of the P/B superlattice is much stronger than that of either of its components. This means that something takes place at the interface. According to our calculation, the MnO_6 elongation along interface normal, defined by the c/a ratio, varies from 14% to 6% as lattice strain ascends from -2% to 4% [Fig. 5(a)]. In contrast, it changes from 6% to -4% for a bare LSMO film across the same strain range [46,47]. The enhanced MnO_6 elongation could be ascribed to the appearance of spared space in the CoO_4 layer that loses two oxygen ions for each tetrahedron compared with CoO_6. More than that, the CoO_4 tetrahedra are distorted and tilted by adjacent MnO_6 octahedra via shared oxygen atoms, deviating by an angle from 21° to 37° (depending on lattice strains) away from the custom z direction. This indicates the occurrence of interfacial reconstruction, i.e., atomic and orbital rearrangement at interface. In Figs. 5(b) and 5(c) we show the distorted MnO_6 and CoO_4 and the corresponding energy level of different orbitals.

By analyzing Eq. (3), we can get the selection rules for preferred spin orientation of transion element ions. As well established, the d states can be represented in terms of $d_m = d_{xy}, d_{yz}, d_{z^2}, d_{xz}, d_{x^2-y^2}$, standing for the d orbital states with the magnetic quantum number $m = -2, -1, 0, 1, 2$ respectively. Hence, the preferred spin orientation can be

depicted using the minimum difference $|\Delta L_Z|$ in the magnetic quantum numbers. For example, for two states with identical spin, if $|\Delta L_Z| = 2$, these two d states cannot interact under SOC; if $|\Delta L_Z| = 1$, preferred spin orientation would be perpendicular to the z direction; if $|\Delta L_Z| = 0$, the preferred spin orientation is parallel to the z direction [48].

As depicted in Fig. 5(b), Mn^{3+} ion in a z-elongated MnO_6 octahedron has the spin configuration $(d_{xz/yz\uparrow})^1 (d_{xy\uparrow})^1 (d_{z^2\uparrow})^1 (d_{x^2-y^2\uparrow})^0$. The lowest energy difference occurs between the $d_{z^2\uparrow}$ and $d_{x^2-y^2\uparrow}$ levels. However, this orbital pair cannot interact through SOC because $|\Delta L_Z| = 2$. The next lowest energy difference occurs between $d_{xy\uparrow}$ and $d_{x^2-y^2\uparrow}$, and the corresponding spin orientation will be parallel to the z axis since $|\Delta L_Z| = 0$. Similarly, the interaction between $d_{z^2\uparrow}$ and unoccupied $d_{xz/yz\downarrow}$ also gives rise to a positive contribution to MAE since $|\Delta L_Z| = 1$. After direction calculations, we can get a quantitative expression of MAE for Mn ions without orbital mixing,

$$\text{MAE} = \xi^2 \left(\frac{1}{\Delta_1} + \frac{1}{4\Delta_2} \right), \tag{4}$$

where Δ_1 and Δ_2 are the energy difference between the occupied and unoccupied orbitals of $d_{x^2-y^2\uparrow}$ and $d_{xy\uparrow}$ and $d_{z^2\uparrow}$ and $d_{xz/yz\downarrow}$, respectively. According to Eq. (4), either component of the MAE will be positive, in sharp contrast to the results of Fig. 3. This inconsistence reveals the important role of orbital hybridization in determining magnetic anisotropy. In fact, if the occupied/unoccupied e_g orbitals are mixed states of the $d_{x^2-y^2}$ and d_{z^2} orbtials, negative terms such as $\langle d_{x^2-y^2\downarrow}|\hat{L}_z|d_{xy\uparrow}\rangle$ and $\langle d_{yz\uparrow}|\hat{L}_z|d_{z^2\downarrow}\rangle$ could be introduced into Eq. (4). Take the $d_{x^2-y^2}$-d_{xy} orbital pair as an example. The energy difference between occupied $d_{x^2-y^2\uparrow}$ and unoccupied $d_{xy\downarrow}$ is smaller than that between occupied $d_{xy\uparrow}$ and unoccupied $d_{x^2-y^2\uparrow}$ (shown by $\Delta_1^{\uparrow\uparrow}$ and $\Delta_1^{\uparrow\downarrow}$, respectively, in Fig. 4), i.e., the former negative term is larger in magnitude than the latter, positive one. As a result, the $\langle d_{xy}|\hat{L}_z|d_{x^2-y^2}\rangle$ term is negative. Therefore, the symmetry mismatch of the heterostructure provides a feasible approach towards orbital mixing, giving rise to an effective tuning to magnetic anisotropy.

Although the MnO_6 octahedron tilted away from the global z direction with an angle about 5° to 9° as strain grows from -2% to $+4\%$, this small tilt does not change our main results about PMA as its error is smaller by two orders of magnitude than the MAE value. It is therefore plausible to ascribe the anomalous PMA of the Mn ion in superlattice to the z-axis elongation of MnO_6.

In contrast, the Mn^{3+} ion in a z-contracted MnO_6 octahedron owns a spin configuration of $(d_{xy\uparrow})^1 (d_{xz/yz\uparrow})^1 (d_{x^2-y^2\uparrow})^1 (d_{z^2\uparrow})^0$. In this case, $|\Delta L_Z| = 1$ occurs between $d_{xz/yz\uparrow}$ and $d_{z^2\uparrow}$ levels which have the next lowest energy difference. Hence the preferred spin orientation is perpendicular to the z direction, i.e., the ion will show an easy-plane anisotropy. This is consistent with our calculations for the bare LSMO film at the $+4\%$ strain state and also the previous experiments [12].

Different from Mn, a Co^{2+} ion in an ideal CoO_4 tetrahedron has the $(d_{x^2-y^2})^2 (d_{z^2})^2 (d_{xy})^1 (d_{xz/yz})^1$ spin configuration

[Fig. 5(c)]. It is easy to see that the two orbitals with lowest energy difference are $d_{x^2-y^2\downarrow}$ and $d_{xy\downarrow}$ ($d_{z^2\downarrow}$ and $d_{xy\downarrow}$ cannot interact via SOC as their L_Z values differ by 2). Since these two levels have the same $|m|$ value, their interaction leads to a maximal energy gain when the spin aligns in parallel to the z direction, i.e., a positive SOC term $\langle d_{x^2-y^2\downarrow}|\hat{L}_z|d_{xy\downarrow}\rangle$. Because of the hybridization between the Co $3d$ and O $2p$ orbitals both the spin-down e_g and t_{2g} orbtials are partially occupied, yielding a positive $\langle d_{xz\downarrow}|\hat{L}_z|d_{yz\downarrow}\rangle$ term. This term is closely related to orbital hybridization. It is therefore very sensitive to lattice strains, nearly halved from $\varepsilon = -2\%$ to $+4\%$. Based on the selection rule mentioned above, we can get three additional smaller terms $\langle d_{x^2-y^2\downarrow}|\hat{L}_z|d_{yz\downarrow}\rangle$, $\langle d_{z^2\downarrow}|\hat{L}_z|d_{yz\downarrow}\rangle$, and $d_{xy\downarrow}|\hat{L}_z|d_{xz\downarrow}$. These matrix elements are all negative as $|\Delta L_Z| = 1$ and less susceptable to lattice strains.

Similarly, we can conclude that the spin of octahedron-coordinated Co^{2+} is perpendicular to the z direction, i.e., easy-plane anisotropy. Thus, the magnetic anisotropy in LCO is the competition between the octahedron-coordinated and tetrahedron-coordinated Co^{2+}. This result tells us the probability of modulating magnetic anisotropy [32,49] through modifying the chemical environment of a Co atom in tetrahedral and octahedral coordination.

IV. SUMMARY

Based on density functional theory calculations, we performed a systematic investigation on magnetic anisotropy for a perovskite/brownmillerite-type $La_{1/2}Sr_{1/2}MnO_3/LaCoO_{2.5}$ interface, which is modeled by a brownmillerite-structured superlattice consisting of $(CoO_4)_1/(MnO_6)_1$ with the A-site atom of La for the CoO_4 layer and half La and half Sr for the MnO_6 layer. A PMA up to 1.9×10^7 erg/cm^3 is obtained under the compressive strain of -2%. As lattice strains transit from the compressive to the tensile state, PMA displays a smooth decrease but remains as large as 1×10^7 erg/cm^3 under a tensile strain of $+4\%$. The most remarkable result is that the MnO_6 layer and the CoO_4 layer have comparable contributions to PMA and, moreover, the PMA is much larger than that of either component of the superlattice, due to interface reconstruction that leads to strong orbital hybridization. We identified the orbital pairs that strongly affect magnetic anisotropy and show that adjusting orbital mixing is an effective approach to tune magnetic anisotropy. The present work may inspire further experimental and theoretical explorations to manipulate magnetic anisotropy, which is highly desired by highly efficient spintronic applications.

[1] S. Mangin, D. Ravelosona, J. A. Katine, M. J. Carey, B. D. Terris, and E. E. Fullerton, Nat. Mater. **5**, 210 (2006).

[2] S. Ikeda, K. Miura, H. Yamamoto, K. Mizunuma, H. D. Gan, M. Endo, S. Kanai, J. Hayakawa, F. Matsukura, and H. Ohno, Nat. Mater. **9**, 721 (2010).

[3] L. Liu, C.-F. Pai, Y. Li, H. W. Tseng, D. C. Ralph, and R. A. Buhrman, Science **336**, 555 (2012).

[4] S. Emori, U. Bauer, S.-M. Ahn, E. Martinez, and G. S. D. Beach, Nat. Mater. **12**, 611 (2013).

[5] H. Bethe, Ann. Phys. (Berlin) **395**, 133 (1929).

[6] C. J. Ballhausen, *Introduction to Ligand Field Theory* (McGraw-Hill, New York, 1962).

[7] L. Néel, J. Phys. Radium **15**, 225 (1954).

[8] M. T. Johnson, R. Jungblut, P. J. Kelly, and F. J. A. den Broeder, J. Magn. Magn. Mater. **148**, 118 (1995).

[9] D. Yi, J. Liu, S.-L. Hsu, L. Zhang, Y. Choi, J.-W. Kim, Z. Chen, J. D. Clarkson, C. R. Serrao, E. Arenholz *et al.*, Proc. Natl. Acad. Sci. USA **113**, 6397 (2016).

[10] A. Urushibara, Y. Moritomo, T. Arima, A. Asamitsu, G. Kido, and Y. Tokura, Phys. Rev. B **51**, 14103 (1995).

[11] A. M. Haghiri-Gosnet, J. Wolfman, B. Mercey, Ch. Simon, P. Lecoeur, M. Korzenski, and M. Hervieu, J. Appl. Phys. **88**, 4257 (2000).

[12] C. Kwon, M. C. Robson, K.-C. Kim, J. Y. Gu, S. E. Lofland, S. M. Bhagat, Z. Trajanovic, M. Rajeswari, T. Venkatesan, A. R. Kratz *et al.*, J. Magn. Magn. Mater. **172**, 229 (1997).

[13] Z. Liao, M. Huijben, Z. Zhong, N. Gauquelin, S. Macke, R. J. Green, S. Van Aert, J. Verbeeck, G.Van Tendeloo, K. Held *et al.*, Nat. Mater. **15**, 425 (2016).

[14] J. Zhang, Z. Zhong, X. Guan, X. Shen, J. Zhang, F. Han, H. Zhang, H. Zhang, X. Yan, Q. Zhang *et al.*, Nat. Commun. **9**, 1923 (2018).

[15] P. E. Blöchl, Phys. Rev. B **50**, 17953 (1994).

[16] G. Kresse and J. Furthmüller, Phys. Rev. B **54**, 11169 (1996).

[17] G. Kresse and D. Joubert, Phys. Rev. B **59**, 1758 (1999).

[18] J. P. Perdew, K. Burke, and M. Ernzerhof, Phys. Rev. Lett. **77**, 3865 (1996).

[19] J. P. Perdew, A. Ruzsinszky, G. I. Csonka, O. A. Vydrov, G. E. Scuseria, L. A. Constantin, X. Zhou, and K. Burke, Phys. Rev. Lett. **100**, 136406 (2008).

[20] See Supplemental Material at http://link.aps.org/supplemental/10.1103/PhysRevB.100.144413 for details about *k*-point convergence test, the MAE results at more complex (3,3) *P/B* interface and that calculated by force theorem, orbital occupation comparison, band structures with different magnetization orientations, and projected density of states of Mn and Co ions.

[21] V. I. Anisimov, J. Zaanen, and O. K. Andersen, Phys. Rev. B **44**, 943 (1991).

[22] Z. Cai, Y. Kuru, J. Woo Han, Y. Chen, and B. Yildiz, J. Am. Chem. Soc. **133**, 17696 (2011).

[23] Q. Zhang, S. Dong, B. Wang, and S. Yunoki, Phys. Rev. B **86**, 094403 (2012).

[24] D. Hobbs, G. Kresse, and J. Hafner, Phys. Rev. B **62**, 11556 (2000).

[25] M. Marsman and J. Hafner, Phys. Rev. B **66**, 224409 (2002).

[26] V. Antropov, L. Ke, and D. Aberg, Solid State Commun. **194**, 35 (2014).

[27] J. Zhang, P. V. Lukashev, S. S. Jaswal, and E. Y. Tsymbal, Phys. Rev. B **96**, 014435 (2017).

[28] R. Skomski, A. Kashyap, and A. Enders, J. Appl. Phys. **109**, 07E143 (2011).

[29] A. Muñoz, C. de la Calle, J. A. Alonso, P. M. Botta, V. Pardo, D. Baldomir, and J. Rivas, Phys. Rev. B **78**, 054404 (2008).

[30] D. Böttcher and J. Henk, J. Phys.: Condens. Matter **25**, 136005 (2013).

[31] M. Ziese, I. Vrejoiu, E. Pippel, P. Esquinazi, D. Hesse, C. Etz, J. Henk, A. Ernst, I. V. Maznichenko, W. Hergert *et al.*, Phys. Rev. Lett. **104**, 167203 (2010).

[32] J. Y. Ni, P. S. Wang, J. L. Lu, and H. J. Xiang, Phys. Rev. Lett. **122**, 117601 (2019).

[33] S. Hu, C. Cazorla, F. Xiang, H. Ma, J. Wang, J. Wang, X. Wang, C. Ulrich, L. Chen, and J. Seidel, ACS Appl. Mater. Interfaces **10**, 22348 (2018).

[34] K. Steenbeck, T. Habisreuther, C. Dubourdieu, and J. P. Sénateur, Appl. Phys. Lett. **80**, 3361 (2002).

[35] J. Dubowik, Phys. Rev. B **54**, 1088 (1996).

[36] G. H. O. Daalderop, P. J. Kelly, and M. F. H. Schuurmans, Phys. Rev. B **41**, 11919 (1990).

[37] X. Wang, D.-S. Wang, R. Wu, and A. J. Freeman, J. Magn. Magn. Mater. **159**, 337 (1996).

[38] G. H. O. Daalderop, P. J. Kelly, and M. F. H. Schuurmans, Phys. Rev. B **50**, 9989 (1994).

[39] S. Ouazi, S. Vlaic, S. Rusponi, G. Moulas, P. Buluschek, K. Halleux, S. Bornemann, S. Mankovsky, J. Minár, J. B. Staunton, H. Ebert *et al.*, Nat. Commun. **3**, 1313 (2012).

[40] X. Wang, R. Wu, D.-S. Wang, and A. J. Freeman, Phys. Rev. B **54**, 61 (1996).

[41] D. S. Wang, R. Wu, and A. J. Freeman, Phys. Rev. B **47**, 14932 (1993).

[42] P. Bruno, Phys. Rev. B **39**, 865 (1989).

[43] E. Francisco and L. Pueyo, Phys. Rev. A **36**, 1978 (1987).

[44] C. Andersson, B. Sanyal, O. Eriksson, L. Nordström, O. Karis, D. Arvanitis, T. Konishi, E. Holub-Krappe, and J. H. Dunn, Phys. Rev. Lett. **99**, 177207 (2007).

[45] Gerrit van der Laan, J. Phys.: Condens. Matter **10**, 3239 (1998).

[46] A. Tebano, C. Aruta, P. G. Medaglia, F. Tozzi, G. Balestrino, A. A. Sidorenko, G. Allodi, R. De Renzi, G. Ghiringhelli, C. Dallera, L. Braicovich, and N. B. Brookes, Phys. Rev. B **74**, 245116 (2006).

[47] S. Hausmann, J. Ye, T. Aoki, J.-G. Zheng, J. Stahn, F. Bern, B. Chen, C. Autieri, B. Sanyal, P. D. Esquinazi *et al.*, Sci. Rep. **7**, 10734 (2017).

[48] M.-H. Whangbo, E. E. Gordon, H. Xiang, H.-J. Koo, and C. Lee, Acc. Chem. Res. **48**, 3080 (2015).

[49] N. Lu, P. Zhang, Q. Zhang, R. Qiao, Q. He, H.-B. Li, Y. Wang, J. Guo, D. Zhang, Z. Duan *et al.*, Nature (London) **546**, 124 (2017).